Cluster and Velocity Effects on Yields and Kinetic Energy Distributions of Li^+ Desorbed from LiF

J. A. M. Pereira and E. F. da Silveira

Departamento de Física, Pontifícia Universidade Católica, CP 38071, Rio de Janeiro 22952-970, Brazil

(Received 30 August 1999)

MeV N^+ and N_2^+ ions were used to induce Li^+ desorption from LiF. The contributions due to elastic atomic collisions and electronic excitation processes to the sputtering yield could be unambiguously separated. In the case of N_2^+ ions, a Li^+ yield enhancement, i.e., $Y(N_2^+) > 2Y(N^+)$, was found only for the electronic process. The maximum sputtering yield was observed in a projectile velocity range where the projectile electronic energy loss still increases. These results are simultaneously explained using the radial distribution of the deposited energy rather than the electronic energy loss.

PACS numbers: 79.20.Rf, 61.80.Lj

The collision of a fast heavy ion in a solid produces a variety of nonequilibrium events; among them one observes the ejection of neutral or ionized particles from the surface. This phenomenon, known as sputtering, results from two different mechanisms: the particle emission originated from atomic collision cascades (nuclear sputtering) [1] and, a more subtle mechanism, the one where the emission process is initiated by electronic excitations (electronic sputtering) [2]. The knowledge of the sputtering is important for a general understanding of the effects caused by the deposition and the diffusion of energy in solids following penetration of swift heavy ions. The formation of ion tracks in the target sample is a related phenomenon which has received attention from a technological point of view [3]. Track registration is important for the controlled pinning of flux lines in high-T_c superconductors, for instance [4]. The electronic sputtering became of particular interest for biochemistry because it permits, in conjunction with time-of-flight spectroscopy, the identification of large organic nonvolatile molecules, as, for example, bleomycin and amphotericin [5]. Electronic sputtering is also relevant in astrophysics. The surfaces of certain solar system bodies, like the moons of the outer planets, are constantly bombarded by MeV ions causing particle emission. The sputtered particles trapped by the local gravity form tenuous atmospheres. The prediction of the electronic sputtering yield and the desorbed particles kinetic energy distribution is important to estimate the gas content in such atmospheres and to evaluate the lifetime of planetary rings [6]. So far, there is no consistent theory to explain electronic sputtering.

Sputtering from insulating surfaces induced by atomic and molecular projectiles having velocities around the Bohr velocity is investigated in this work. The electronic and nuclear sputtering yields are comparable in this velocity range. It has been shown that the relative contribution of these processes can be obtained using the kinetic energy distribution of the emitted ions [7]. The linear cascade theory can be applied to describe the nuclear sputtering contribution. This theory predicts the proportionality between the emission yield and the nuclear energy loss, S_n, and also the shape of the energy distribution curve. Many models predict that the desorption yield due to electronic sputtering is proportional to the square of the electronic energy loss, S_e, but in several cases significant deviations from the S_e^2 law have been noted [8,9].

The energy deposited by a MeV atomic projectile to the surface region ($\sim$1 keV in the first nm below the surface) is deposited over a small volume ($\sim 1\ \mathrm{nm}^3$) in a short time ($\sim 10^{-17}$ s). A correlation between the deposited energy and the desorption yield is expected. However, it is observed that for the same amount of deposited energy, faster atomic projectiles produce smaller desorption yields. This is the so-called *velocity effect* [8–10]. For cluster projectiles, the energy loss inside the solid is enhanced as a result of the spatial and temporal correlation during the impact. This effect leads to very high values of the deposited energy density [11,12] and, consequently, nonlinear effects are likely to occur. This *cluster effect* is usually described in terms of the yield enhancement factor

$$R = Y(n)/nY(1), \tag{1}$$

where n is the number of atomic constituents in the cluster projectile and Y represents the yield of a given secondary ion measured at the same projectile velocity. The cluster effect ($R \neq 1$) is well established for the secondary particle emission yield due to nuclear and electronic sputtering processes [13–15]. However, there are no experimental data available for kinetic energy distributions of the emitted ions due to cluster impact. Only recently the cluster effect on kinetic energy distributions has been experimentally investigated [16].

In this Letter, a connection between cluster and velocity effects is made. They are analyzed simultaneously using the radial distribution of the deposited energy. The aim is to obtain a common explanation for both effects and describe them quantitatively using the same model. A semiempirical law, able to predict the variation of the electronic sputtering yield with the projectile velocity with good accuracy, is derived.

 0031-9007/00/84(25)/5904(4)$15.00

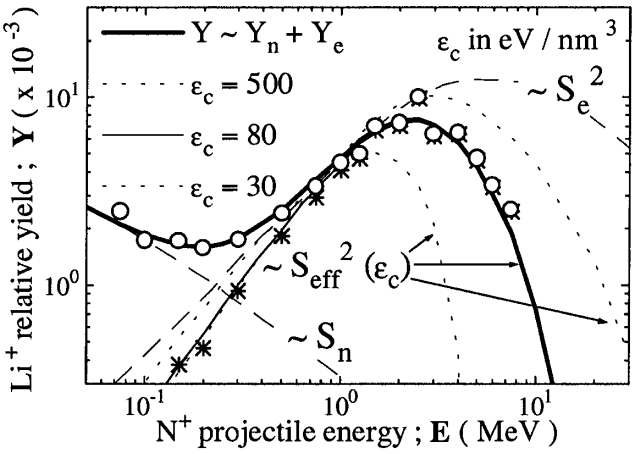

FIG. 1. Li^+ desorption yields, not corrected for experimental efficiency (○), and the corresponding electronic sputtering yield fraction (∗). The S_{eff}^2 curves, with adequate normalizations (solid and dotted lines), are shown for three ε_c values (see text). The total yield is given by $Y = A_n S_n + A_e S_{\text{eff}}^2$ (heavy solid line). The electronic and the nuclear energy loss variations (dashed lines) are indicated by the symbols S_e^2 and S_n, respectively.

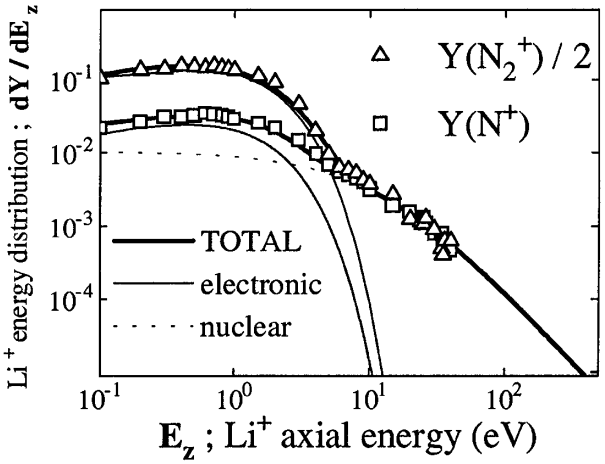

FIG. 2. Axial energy distributions of Li^+ secondary ions for N^+ (0.2 MeV) and N_2^+ (0.4 MeV) ion impact. The nuclear and electronic energy distributions are described by $A_n(E_z + U)^{-2}$ (see Ref. [7]) and by $A_e E_z^{\alpha} \exp(-\beta E_z)$, respectively. The constants $\alpha = 0.4$ and $\beta = 0.9$ are the same for both cases. The heavy solid lines represent the sum of the two contributions.

A description of the time-of-flight experimental setup used for the present measurements is found in Ref. [7]. It is important to mention that the experiments are performed in an event-by-event basis and that the number of primary ion impacts per unit area on the surface needed to obtain each spectrum is as low as 10^7 cm^{-2}. Therefore, target material properties remain unchanged. The simple electronic and geometrical properties of lithium fluoride help the understanding of the Li^+ emission process [16,17].

The open circles in Fig. 1 represent the obtained relative Li^+ desorption yield, Y, measured as a function of the N^+ projectile energy, E. The nuclear energy loss (S_n) and the square of the electronic energy loss (S_e^2), normalized to the yield data, are also represented. In a first order approximation, it was considered that the nuclear and electronic sputtering mechanisms act independently. Therefore, the total secondary ion yield is roughly written as the sum of the nuclear and electronic contributions: $Y \sim Y_n + Y_e$. From the linear cascade theory one has $Y_n = A_n S_n$. The electronic sputtering contribution (stars) is obtained by subtracting the nuclear sputtering yield fraction, Y_n, from the measured yield. This is done according to the energy distribution measurement as will be seen in the next paragraphs.

At low projectile energies ($E < 0.3$ MeV), the nuclear sputtering contribution dominates. At high energies, one observes the velocity effect on the electronic sputtering. As shown in Fig. 1, the S_e^2 prediction agrees reasonably well with the data for $E < 2.0$ MeV ($A_e S_e^2 = Y_e$) but strongly overestimates the Li^+ yield ($A_e S_e^2 > Y_e$) for higher projectile energies.

The Li^+ secondary ion energy distributions due to atomic and molecular projectiles at 0.2 MeV/atom are shown in Fig. 2. In the case of N_2^+ projectiles the yield distribution (dY/dE_z) is divided by a factor of 2. The nuclear sputtering mechanism is responsible for the high energy tail of the distributions ($E_z > 10$ eV) in both cases. The contribution of this mechanism is evaluated using an extension of the linear collision cascades theory for ionic solids (dotted line) [7]. The predicted values, normalized to the high E_z tail, are then subtracted from the total energy distribution (data points) to obtain the energy distribution due to the electronic sputtering (solid lines). Following this procedure, it is possible to decompose the desorption yield into the electronic and the nuclear sputtering contributions. The relative yields due to each process are shown in Table I. It is worth mentioning that atomic and molecular projectiles produce the same Li^+ characteristic emission energies in spite of the deposited energy density increase achieved with the N_2^+ impact. This fact is related to the electronic sputtering mechanism of Li^+ secondary ions [16]. It is also important to notice that the sum $Y \sim Y_n + Y_e$ describes surprisingly well the yield dependence of the projectile energy (Fig. 1) as well as the energy distributions (Fig. 2). This would imply that nuclear and electronic sputtering act in different time scales.

The collision cascade contribution exhibits no cluster effect, i.e., $Y_n(N_2^+) = 2Y_n(N^+)$. This follows from the additivity of the energy loss due to nuclear collisions $S_n(N_2^+) = 2S_n(N^+)$. The additivity rule applied to the electronic energy loss cannot reproduce the data for electronic sputtering. If one considers $S_e(N_2^+) = 2S_e(N^+)$

TABLE I. Li^+ yields for N^+ and N_2^+ ions at 0.20 MeV/atom.

Primary ion	Nuclear	Electronic	Total
N^+	1.10	0.45	1.55
N_2^+	2.20	5.38	7.58

and $Y_e = A_e S_e^2$ (since the measurement was done for $E = 0.20$ MeV/atom where $A_e S_e^2$ is supposed to be valid), the yield for N_2^+ impact would be 4 times the yield due to N^+ projectiles ($R = 2$). In contrast, a yield enhancement factor of $R = 5.38/(2 \times 0.45) \sim 6$ is found for the electronic sputtering contribution. This new finding shows that the agreement of the law $Y_e = A_e S_e^2$ with the data, for projectile energies lower than the one corresponding to the maximum yield ($E < 2.0$ MeV), is acceptable only for atomic projectiles. A new function, able to include cluster projectiles effects, should be used.

The observed cluster and velocity effects on the electronic sputtering yields can be analyzed using the deposited energy density, $\varepsilon(r, v)$, concept. This quantity depends on the ion velocity v through the infratrack and ultratrack characteristic radii, $r_i < r_u$, and on its electronic energy loss S_e. The Bohr adiabatic radius is usually taken as a good value for r_i which is a measure of the maximum impact parameter for the projectile to perform ionizations and/or excitations. The infratrack region is defined by $r < r_i$. The ion-electron collision kinematics and secondary electron range in solids are used to define r_u [9,18,19]. Consequently, one has that $r_u = r_u(v)$ and at a given projectile velocity, atomic and molecular ions deposit their energy into the same track volume.

In order to perform analytical calculations, the function

$$\varepsilon(r, v) = \varepsilon_0(v)/[1 + (r/r_i)^2] \qquad (2)$$

was used in this work to approximate the energy density inside the track volume. For $r > r_u(v)$ the function $\varepsilon(r, v)$ is set to zero since the electrons ejected from the infratrack cannot deposit their energy in regions beyond the ultratrack boundary. In the intermediate region the proposed function has the expected $1/r^2$ behavior [3,9]. The energy density at $r = 0$, $\varepsilon_0(v)$, is determined, integrating Eq. (2) over all space and equating the result to the electronic energy loss as in $S_e(v) = \int_0^\infty 2\pi r \varepsilon(r, v)\, dr$. Figure 3 shows schematically the energy density function for two atomic ion velocities $v_1 < v_2$. These velocities are such that $S_e(v_1) = S_e(v_2)$. For low ion velocities, the deposited energy is more concentrated near the ion path since the secondary electron cascades have smaller transversal ranges than those corresponding to high velocities. The parameter ε_c, appearing in Figs. 1 and 3, is a critical energy density for ion emission which depends on the target material [12]. It defines a critical radius, r_c, such that $\varepsilon(r_c, v) = \varepsilon_c$. In the region defined by $r < r_c$, or equivalently $\varepsilon(r) > \varepsilon_c$, the atomic bonds are broken by the secondary electron cascades permitting the ions to be released from the surface. An effective energy deposition per unit path for ion desorption, S_{eff}, is defined by integrating $\varepsilon(r)$ inside the area limited by the critical radius ($r < r_c$). The calculation gives

$$S_{\text{eff}} = S_e \ln(\varepsilon_0/\varepsilon_c)/\ln[1 + (r_u/r_i)^2]. \qquad (3)$$

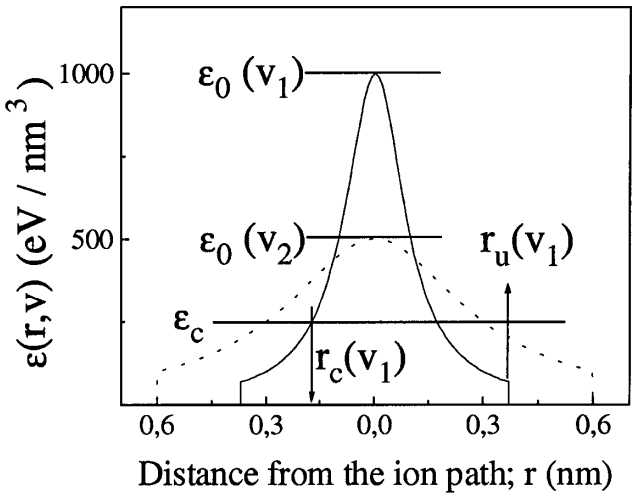

FIG. 3. The energy density approximated by a Lorentzian for two projectile velocities $v_1 < v_2$. The ε_c value is characteristic of the secondary ion and target material. The critical radius r_c is a function of the projectile velocity. One has that $r_i \sim v$ and $r_u \sim v^2$ [9].

This function is used to fit the Y_e data in Fig. 1 by using ε_c as a free parameter. It is possible to describe the Li^+ yield using the law $Y_e = A_e S_{\text{eff}}^2$, letting $\varepsilon_c = 80$ eV/nm^3, over the whole projectile energy range. A good description of the total yield is given by $Y = A_n S_n + A_e S_{\text{eff}}^2$ (Fig. 1). The ε_c value of 80 eV/nm^3 corresponds to an average energy density of 3 eV/atom and is similar to the values found in Ref. [12] which were obtained from track diameter measurements and not from sputtering yield measurements. The velocity effect is thus explained in terms of the deposited energy density which takes into account the variation of the energy deposition volume with the projectile velocity.

The electronic energy loss of N_2^+ projectiles was obtained considering the following models: (i) the linear approximation given by $S_e(N_2^+) = 2 \times S_e(N^+)$ and (ii) the united atom limit which considers the N_2^+ projectile as a single ion with double nuclear charge and the same number of electrons. This limit can be regarded as the monopole term of a multipole expansion of the molecular ion energy loss [20]. For $E = 0.20$ MeV/atom, the united atom limit predicts $S_e(N_2^+) = 2 \times 0.88 \times S_e(N^+)$. Once the cluster energy loss is known, the calculation of the yield enhancement factor is done considering the law $Y_e = A_e S_{\text{eff}}^2$ and using Eq. (1). The results are shown in Fig. 4 as a function of the ratio $\varepsilon_c/\varepsilon_0(N^+)$. The experimental point corresponds to $\varepsilon_c = 80$ eV/nm^3 consistently with the information of all data points in Fig. 1. It is seen that, within the effective energy deposition formalism, both limits for the cluster energy loss produce yield enhancement factors larger than two as experimentally observed. Moreover, the experimental value of R measured for the electronic contribution of Li^+ lies in between the two limiting cases.

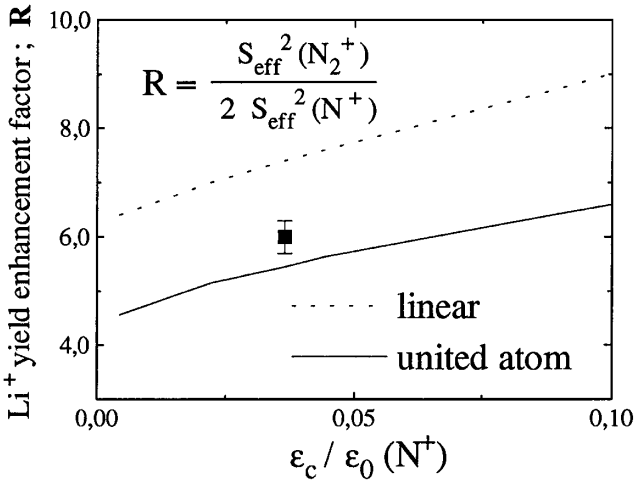

FIG. 4. Enhancement factors evaluated using the function S_{eff}. The linear (upper limit) and united atom (lower limit) approximations were used to calculate molecular ion energy loss. The ε_c value for the measurement is 80 eV/nm^3. For $E = 0.20$ MeV/atom one has $\varepsilon_0(\text{N}^+) = 2.26 \times 10^3$ eV/nm^3. The error bar corresponds to the statistical error (5%).

Nonlinear effects were found for the electronic sputtering of Li^+ secondary ions from LiF. The effective energy deposition formalism consistently describes the experimentally observed cluster and velocity effects. Even the sublinear cluster ion energy loss in the united atom limit furnishes a supralinear yield enhancement factor. This fact shows the importance of considering the energy density, together with the electronic energy loss, as a primary parameter to describe the desorption process.

The Volkswagen Foundation and the Brazilian agency CNPq are acknowledged for financial support. Many thanks are due to Professor I. S. Bitensky and Professor K. Wien for enlightening discussions.

[1] P. Sigmund, Nucl. Instrum. Methods Phys. Res., Sect. B **27**, 1 (1987).
[2] R. E. Johnson and J. Schou, Mat. Fys. Medd. K. Dan. Vidensk. Selsk. **43**, 403 (1993).
[3] R. Spohr, *Ion Track and Microtechnology* (Vieweg & sohn Verlagsgesellschaft mbH, Braunschweig, 1990).
[4] W. Jiang *et al.*, Phys. Rev. Lett. **72**, 550 (1994).
[5] R. D. Macfarlane, in Proceedings of the Conference Desorption '98 [Braz. J. Phys. **29**, 415 (1999)].
[6] R. E. Johnson, Rev. Mod. Phys. **68**, 305 (1996).
[7] J. A. M. Pereira and E. F. da Silveira, Surf. Sci. **390**, 158 (1997).
[8] W. L. Brown *et al.*, Nucl. Instrum. Methods Phys. Res. **198**, 1 (1982), and references therein.
[9] P. Håkansson, Mat. Fys. Medd. K. Dan. Vidensk. Selsk. **43**, 593 (1993).
[10] A. Albers, K. Wien, P. Dück, W. Treu, and H. Voit, Nucl. Instrum. Methods Phys. Res. **198**, 69 (1982).
[11] H. H. Andersen, Mat. Fys. Medd. K. Dan. Vidensk. Selsk. **43**, 127 (1993).
[12] T. A. Tombrello, Nucl. Instrum. Methods Phys. Res., Sect. B **83**, 508 (1993).
[13] Y. Le Beyec, Int. J. Mass Spectrom. Ion Process. **174**, 101 (1998).
[14] M. Salehpour, D. L. Fishel, and J. Hunt, Phys. Rev. B **38**, 12 320 (1988).
[15] H. H. Andersen *et al.*, Phys. Rev. Lett. **80**, 5433 (1998).
[16] J. A. M. Pereira and E. F. da Silveira, Nucl. Instrum. Methods Phys. Res., Sect. B **155**, 206 (1999).
[17] M. Szymonsky, Mat. Fys. Medd. K. Dan. Vidensk. Selsk. **43**, 495 (1993).
[18] C. C. Watson and T. A. Tombrello, Radiat. Eff. **89**, 263 (1985).
[19] I. A. Baranov *et al.*, Sov. Phys. Usp. **31**, 1015 (1988).
[20] P. Sigmund, I. S. Bitensky, and J. Jensen, Nucl. Instrum. Methods Phys. Res., Sect. B **112**, 1 (1996).